Levantine Journal of Applied Sciences, Volume 3(1) (2023) 1-6

Levantine Journal of Applied Sciences

journal homepage: https://www.ljoas.com

What is the reason of size effect on the hardness and reduced modulus of melt-spun Al-12Si-0.5Sb alloy in the indentation test?

Fikret YILMAZ and Fatih YASAR

Department of Physics, Faculty of Science and Art, Tokat Gaziosmanpasa University, Tokat, Turkey

(Orcid: 0000-0002-1835-4961, Orcid: 0000-0001-6005-2257)

Keywords

Al-Si Alloy
Melt Spun
Indentation Size Effect
Korsunsky Model
Nix-Gao Model

ABSTRACT

In this study, the mechanical properties of melt-spun Al-12Si-0.5Sb alloy were analyzed by nanoindentation technique. Scanning electron microscopy observations exhibited that the alloy has a fine-grained eutectic microstructure. Differential scanning calorimetry analysis revealed two exothermic reaction peaks which were identified as supersature Si atoms in Al matrix. In nanoindentation analysis, a series of loads ranging from 0.5 to 300 mN was applied to the alloy surface to obtain load-depth curves. Two mechanical properties, namely hardness and reduced elastic modulus of alloy, were calculated by Oliver-Pharr approach. Mechanical properties exhibited size dependency, which was called indentation size effect. This phenomenon was evaluated by Nix-Gao and Korsunsky models. It was found that the Korsunsky model was compatible with the data and the hardness values obtained from this model were close to the literature values.

1. Introduction

Physical properties of pure metals such as hardness, tensile strength, corrosion resistance, wear behavior, wettability and castability can be modified and improved by alloying with other metals or nonmetals (Alshmri 2012; Farahany et al. 2013). Al-Si alloys have excellent castability, good corrosion and wear resistance, low-cost machinability, ease of recycling and a high strength-to-weight ratio compared to steel. Therefore, it is widely used; in automotive, aerospace and marine applications (Feng et al. 2014; Golovin 2021; Guo et al. 2020, Kordijazi et al. 2020). Due to these superior properties, Al-Si alloys have more than 90% usage area among all cast aluminum alloy groups (Kordijazi et al. 2020). Al can dissolve a maximum of 1.6 wt.% of Si, while Si cannot dissolve any Al. In Al-Si alloys, eutectic solidification occurs when the Si content is approximately 12.6 wt %. Depending on the Si content, Al-Si alloys are divided into three groups: hypoeutectic (< 10 wt.% Si), eutectic (11–13 wt.% Si) and hypereutectic (> 14 wt.% Si) alloys (Farahany et al. 2013; Kordijazi et al. 2020). In Al-Si alloys, the mechanical properties of the alloy depend on its microstructure, composition and solidification conditions. In Al-Si alloys, addition of antimony around 0.1 – 0.5 wt.% provides refining of lamellar eutectic silicon (Muthusamy et al. 2020). The cooling rate is another important factor affecting the microstructure of the Al-Si alloy. The increase in cooling rate during solidification causes refining of the microstructure, increase in chemical homogeneity and solid solubility, formation of metastable crystalline phases and formation of amorphous phases (Okugawa et al. 2022; Shinde and Sahoo 2022). Melt spinning is the most preferred among the rapid solidification methods as it allows both very high cooling rates and the production of large quantities of material (Stroh et al. 2020).

The mechanical properties of a material are important in determining its operating conditions. However, since the thickness of the melt-spinning ribbons is around 20-100 microns, it is difficult to determine the hardness of the ribbons using static hardness devices. In recent years, the nanoindentation method, which has been developed for the mechanical characterization of small-sized materials, namely thin films and micro size particles, has attracted a lot of attention (Uzun et al. 2001; Ergen 2021; Uzun et al. 2018). In indentation test, applied load and the displacement of indenter

* Corresponding author.
Email address: fikretyilmaz79@gmail.com (F. Yilmaz)
http://dx.doi.org/10.56917/ljoas.15

in a material surface are recorded simultaneously (Vijeesh and Prabhu, 2014). Indentation hardness generally tends to decrease with load in metallic materials. This situation is called indentation size effect (ISE) in the literature (Bull 2022). Studies on the ISE effect in melt-spun ribbons are insufficient and need to be clarified.

In the present study, we examined the mechanical properties of the melt-spun ribbon Al-12wt.%Si-0.5wt.%Sb by using nanoindentation technique according to Nix-Gao and Korsunsky models. Thus, we tried to explain what actually caused the ISE effect observed in the melt-spun ribbon.

2. Experimental Procedure

Al – 12 wt.% Si – 0.5 wt% Sb were weighed from the high purity of Al (99.9 wt.% purity), Si (99.999 wt.% purity) and Sb (99.999 wt.% purity) elements. The prepared mixture was firstly melted in a graphite crucible using induction electric furnace. In order to ensure homogeneity, the melted alloy was carefully stirred with a graphite stick. Rapid solidification process was carried out by melt-spinner (Edmund Bühler, Germany) with the wheel linear velocity of 40 m/s and ejection pressure of 250 mbar. The melt-spun ribbon produced is 1 cm in width and 25 μm in thickness (Figure 1).

Figure 1. Melt-spun ribbon.

Thermal analysis was performed with DSC 131 (Seteram) device with temperature ranges of 100-400℃ and ramp of 10℃/min. The surface of the ribbon was grinded by 1000, 1600, 2400 and 4000 mesh of sandpapers and then polished with Al2O3-water suspension applied on cloths. Nanoindentation tests were performed with a nanoindenter device (Bruker), which has ±19.6 μN of force and ± 1 nm of depth resolutions. The tests were carried out under the loads of 0.5, 5, 10, 50, 100, 200 and 300 mN. Atomic force microscope image was obtained with Q-Scope AFM under tapping mode and scanning area of 40x40 μm. Scanning electron microscope (SEM) images were obtained with Leo Evo 40VP device in secondary electron (SE) mode and under 20 kV accelerating potential.

3. Theoretical Bacground

A schematic load-depth (P-h) curve is given in Fig. 2. The correct determination of indentation hardness (H) and elastic modulus (Er) depends on the correct determination of contact depth.

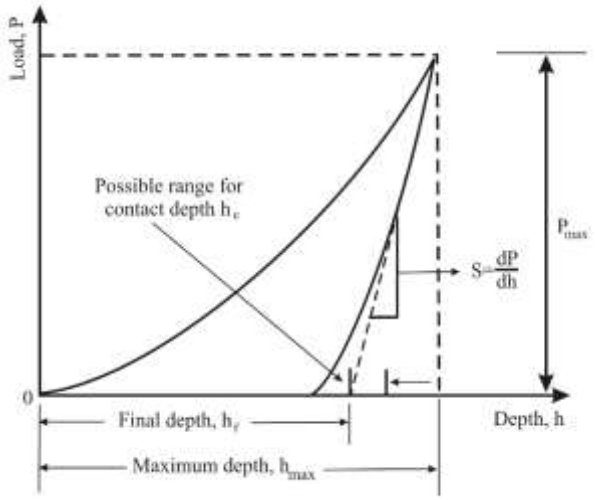

Figure 2. A typical P-h curve shows important indentation parameters.

Oliver and Pharr proposed an easy way to predict the contact depth, which is similar to Sneddon's power law equation for elastic deformations (Oliver and Pharr 1992). Oliver and Pharr showed that power low equation can be fitted to unloading part of P-h curve as follows:

$$P = \alpha\left(h - h_f\right)^m \quad (1)$$

where α and m fitting parameters and hf is final dept after unloading. Thus, contact stiffness (S) can be determined by differentiating the Eq. 1. Then, contact depth (hc) can be calculated with following equation:

$$h_c = h_{max} - \varepsilon\frac{P_{max}}{S} \quad (2)$$

where hmax is maximum depth at peak load and ε is the constant depending on the tip geometry (0.7268 for conical indenters). Once hc is calculated, H and Er can be found with following equations, respectively.

$$H = \frac{P_{max}}{A_c} \quad (3)$$

$$E_r = \beta\frac{\sqrt{\pi}}{2}\frac{S}{\sqrt{A_c}} \quad (4)$$

where Ac is contact area, which is equal to 24.5hc2 and β is 1.034 for Berkovich tip indenter.

In indentation test in some cases hardness tends to increase as the indent size decreases at small depths, which is called indentation size effect (ISE). In literature, size dependency of the hardness can be analyzed by Nix and Gao based on geometrically necessary

dislocations and Korsunsky et al. based on substrate effect in coated systems (Nix and Gao 1998; Korsunsky et al. 1998). According to Nix-Gao model true hardness (H0) can be obtained as follow:

$$H^2 = {H_0}^2 + \frac{{H_0}^2 h^*}{h} \quad (5)$$

where h* is characteristic length, h is contact depth and H is hardness for each load. On the other hand, according to the Korsunsky model ribbon hardness can be obtained as follow:

$$H = \frac{H_F + kH_S\beta^2}{1+k\beta^2} \quad (6)$$

where HF is the film hardness, HS is the substrate hardness, k is the fitting parameter and β is relative depth (hc/t).

3. Results and Discussion

SEM micrographs of the both surfaces of melt-spun ribbon are given in Fig. 3. The ribbon is composed of finely branched eutectic Si network and α-Al phases on both surfaces. The air side of the ribbon has a relatively coarser microstructure compared to its wheel side counterpart, which can be ascribed to lower cooling rate on air side. Tkatch et al. (2002) have reported that cooling rates during melt spinning can be affected by wheel speed, gas ejection pressure and melting temperatures. They also showed that wheel side with higher thermal conductivity than air is responsible for the fine microstructure (Tkatch et al. 2002). Marola et al. (2023) have reported that the solidification conditions change with heat dissipation in the air when the ribbon detaches from the wheel leading to the formation of bimodal microstructure (Marola et al. 2023).

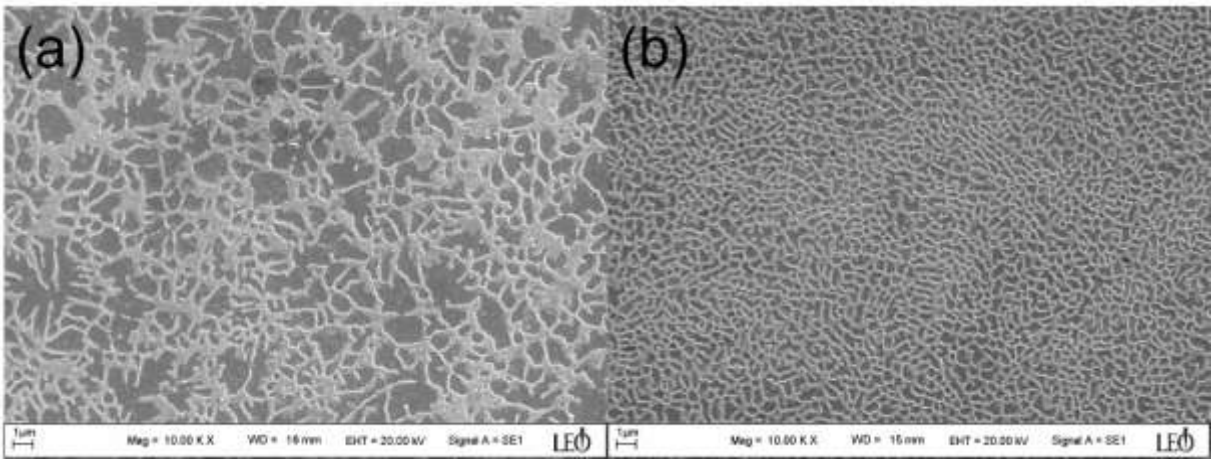

Figure 3. SEM micrographs of ribbon (a) air side (b) wheel side

The DSC heating curve of the ribbon at the temperature range of 100-400℃ is depicted in Fig. 4. Two exothermic peaks appear near 175℃ and 323℃ with the enthalpies of 262 and 159 J/mol, respectively. The first peak indicates the precipitation of Si from supersaturated Al matrix, which is well accepted in literature. Zhang et al. (2007) observed one exothermic peak around 260℃ for Al-7wt%Si-0.4wt%Mg alloy produced with melt-liquid-quenching and water-cooling copper mould techniques (Zhang et al. 2007). It was attributed to the precipitation of Si atoms from Al matrix, which is in consistent with this study. On the other hand, they did not observe the second peak, which can be explained by the slow cooling rate of the techniques they used. In another study, two exothermic peaks, around 285℃ 365℃, were observed in melt-spun Al-8Si-1Sb. The two peaks were attributed to the precipitation of Si and AlSb intermetallic from the supersaturated solid solution, respectively (Karaköse and Keskin 2009). In this study, the second peak observed in DSC trace can be related to precititation of AlSb intermetallic. Moreover, we believe that this peak could be aggregation of precipitation Si atoms. However, more studies are needed to support this view. Load-displacement (P-h) curve of the ribbon at different peak loads is depicted in Fig. 5. All loading part of the curves are overlapping indicating that the sample has homogeneous structure. This result is in agreement with the SEM images.

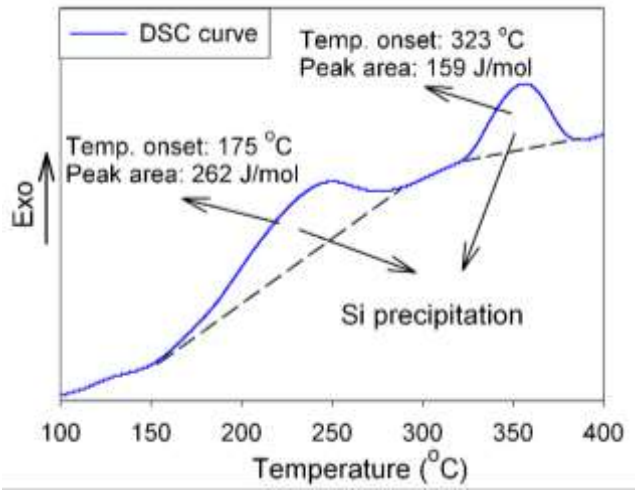

Figure 4. DSC curve of the melt-spun ribbon

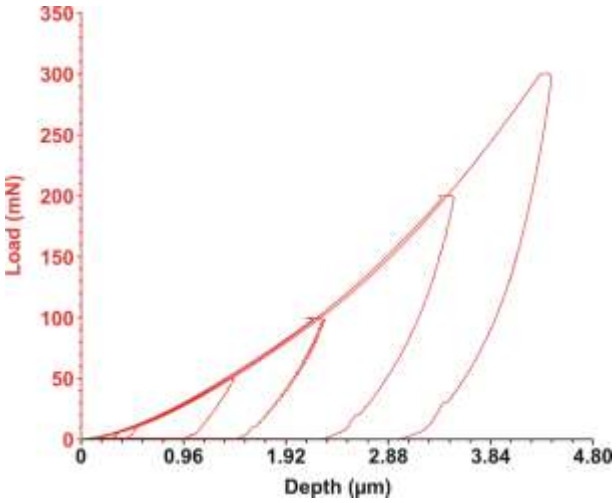

Figure 5. Load-displacement (P-h) curve of the ribbon

Hardness (H) and reduced elastic modulus (Er) of the ribbon calculated by using Eq. 3 and 4 is given in Fig. 6. All values show load dependent behavior, which is called indentation size effect (ISE). The work hardened surface layers, hard surface oxides, contaminants, tip bluntness or poor tip-shape calibrations could all result in the ISE (Li and Warren 1993). The most adopted model developed by Nix and Gao was based on geometrically necessary dislocation underneath a conical indenter (Nix and Gao 1998).

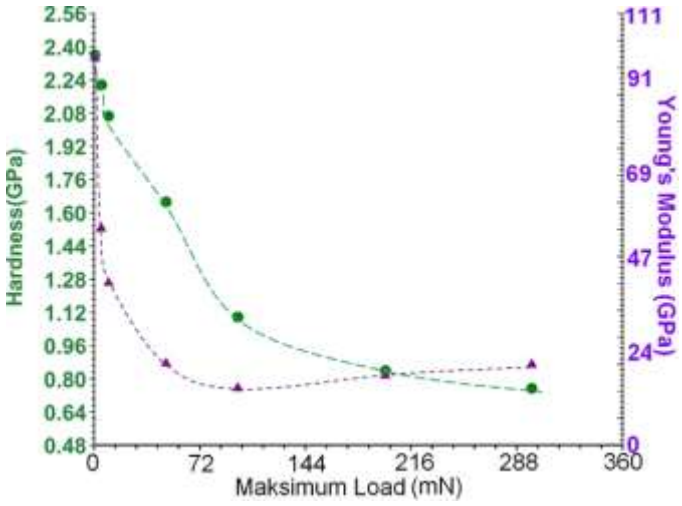

Figure 6. Hardness and reduced modulus variations as a function of maximum loads.

To apply the Nix-Gao model to the ribbon Fig. 7a is obtained by considering the Eq. 5. The hardness is estimated as 1.32 GPa with 0.59 of r2 value. The r2 shows a poor regression line which is not approximating the actual data. Fig. 7b shows the graph obtained using Korsunsky model. In this model, the hardness is estimated as 2.3 GPa with 0.99 of r2 value, which means that the Korsunsky model fits the experimental data better than the Nix-Gao Model. Moreover, the confident and prediction intervals are in the Korsunsky model are quite narrow compared to the Nix-Gao model. This shows that the Korsunsky model is more appropriate in explaining the data compared to the other one. The hardness value calculated from the Korsunsky model is approximately two times higher than the value calculated from the Nix-Gao model. The hardness values of Al-Si alloys vary depending on the modifier elements and production method and take values between 0.7 and 1.6 GPa (Puspitasari et al. 2018; Zeren and Karakulak 2008; Tutunchilar et al. 2012). It is seen that the hardness value obtained from the Nix-Gao model is compatible with these values. On the other hand, these values obtained in the literature belong to the alloys obtained by conventional casting methods where the cooling rate is quite slow. Karaköse and Keskin (2009) have shown that the hardness of melt-spun Al-8Si-1Sb alloy varies from 1.9 and 2.4 GPa, which is consistent with the value obtained from the Korsunsky model. In another study, Abboud et al. (2021) measured the hardness value of 3.25 GPa for the rapidly solidified Al-25wt%Si alloy, which is also close to the hardness calculated from the Korsunsky model. The small difference in hardness may be due to the lower amount of Si in our study. Considering both literature values and fit parameters, it is concluded that Korsunksky model is more successful in explaining the load dependent behavior of hardness.

Korsunsky model was developed primarily for the hardness of coated systems. Although the material analyzed in this study is not a coated system, the ribbon embedded on epoxy can also be considered as a coated system. Here, the ribbon is considered as the coating material, and the epoxy is considered as the substrate. From this point of view, we argue that the size effect observed in hardness is due to the substrate effect rather than geometrically necessary dislocations as Nix-Gao suggested. The decrease of the elastic modulus depending on the applied load is another indicator of the substrate effect. Because the elastic modulus is a distinctive feature for materials, it does not show a load-dependent behavior and depends only on the interatomic bond strength.

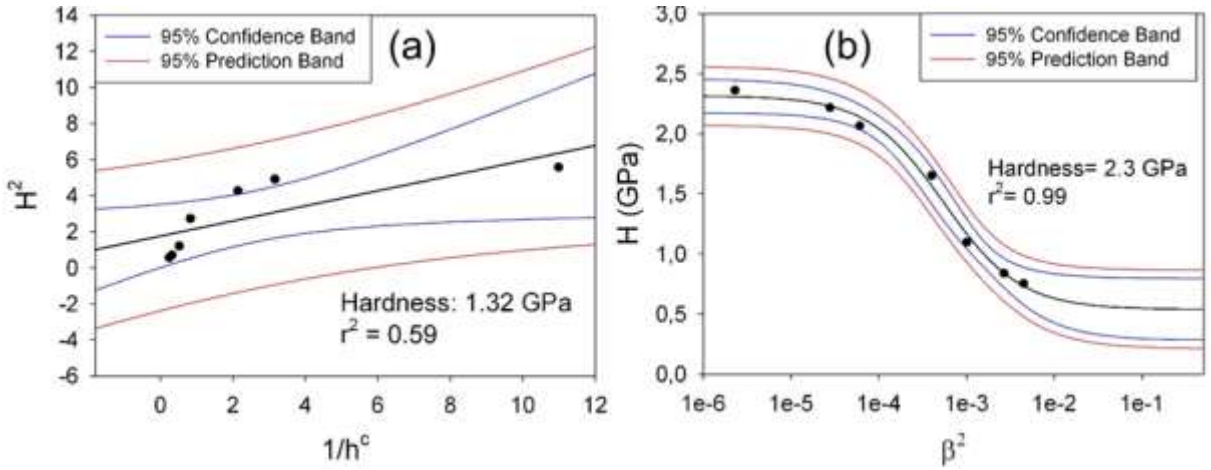

Figure 7. Size-dependent hardness behavior of the ribbon according to the two approaches, (a) Nix-Gao model, (b) Korsunsky model.

4. Conclusion

In this study, we studied mechanical characterization of melt-spun Al-12Si-0.5Sb alloy by nanoindentation test. From SEM observations, we found that the alloy consisted of a very fine Al-Si eutectic structure with a cellular morphology due to high cooling rate of solidification process. Two exothermic peaks seen in the DSC curve were interpreted as an indicator of supersaturation caused by rapid cooling. The hardness and reduced modulus of the alloy exhibited an indentation size effect. We compared the two models, Nix-Gao and Korsunsky, to understand that phenomenon. We found that the Korsunsky model gives more reliable results since it considered substrate effect.

Declaration of Competing Interest

The authors declare that they have no known competing financial interests or personal relationships that could have appeared to influence the work reported in this paper.

Cite this article: *Yilmaz, F., Yasar, F., 2023. What is the reason of size effect on the hardness and reduced modulus of melt-spun Al-12Si-0.5Sb alloy in the indentation test? Levantine Journal of Applied Sciences, Volume 3(1), 1-6.*
http://dx.doi.org/10.56917/ljoas.15

References

Abbound, J.H. and Kayitmazbatir, M., 2022. Microstructural evolution and hardness of rapidly solidified hypereutectic Al-Si surface layers by laser remelting. Advances in Materials and Processing Technologies 8 (4), 4136-4155.

Alshmri, F., 2012. Rapid Solidification Processing: Melt Spinning of Al-High Si Alloys. Advanced Materials Research 383- 390, 1740- 1746. doi:10.4028/www.scientific.net/AMR.383-390.1740

Bull, S.J., 2022. On the origins and mechanisms of the indentation size effect. International Journal of Materials Research 94 (7), 787-792. doi:10.3139/ijmr-2003-0138

Ergen, S., 2021. The effect of indentation temperature and load on mechanical characterization and transformation behavior of high temperature Ti-V-Al-Cu shape memory alloy. Materials Chemistry and Physics 268, 124757. doi:10.1016/j.matchemphys.2021.124757

Farahany, S., Ourdjini, A., Idrsi, M.H. and Shabestari S.G., 2013. Evaluation of the effect of Bi, Sb, Sr and cooling condition on eutectic phases in an Al–Si–Cu alloy (ADC12) by in situ thermal analysis. Thermochimica Acta 559, 59- 68. doi:10.1016/j.tca.2013.02.024

Feng, L., Zhang, H., Wang, Z. and Liu, Y., 2014. Superhydrophobic aluminum alloy surface: Fabrication, structure, and corrosion resistance. Colloids and Surfaces A: Physicochemical and Engineering Aspects 441, 319- 325. doi:10.1016/j.colsurfa.2013.09.014

Golovin, Y.I., 2021. Nanoindentation and Mechanical Properties of Materials at Submicro- and Nanoscale Levels: Recent Results and Achievements. Physics of the Solid State 63 (1), 1–41. doi:10.1134/S1063783421010108

Guo, J., Guan, Z.P., Yan, R.F., Ma, P.K., Wang, M.H., Zhao, P. and Wang, J.G., 2020. Effect of Modification with Different Contents of Sb and Sr on the Thermal Conductivity of Hypoeutectic Al-Si Alloy. Metals 10 (12), 1637-1650. doi:10.3390/met10121637

Karaköse, E., and Keskin, M., 2009. Effect of solidification rate on the microstructure and microhardness of a melt-spun Al–8Si–1Sb alloy. Journal of Alloys and Compounds 479 (1- 2), 230-236. doi:10.1016/j.jallcom.2009.01.006

Kordijazi, A., Behera, S. K., Akbarzadeh, O., Povolo, M. and Rohatgi, P., 2020. A Statistical Analysis to Study the Effect of Silicon Content, Surface Roughness, Droplet Size and Elapsed Time on Wettability of Hypoeutectic Cast Aluminum–Silicon Alloys. The Minerals, Metals & Materials Series: Light Metals 2020, 185- 193. doi:10.1007/978-3-030-36408-3_26

Kordijazi, A., Behera, S. K., Suri, S., Wang, Z., Povolo, M., Salowitz, N., & Rohatgi, P., 2020. Data-driven modeling of wetting angle and corrosion resistance of hypereutectic cast Aluminum-Silicon alloys based on physical and chemical properties of surface. Surfaces and Interfaces 20 (100549). doi:10.1016/j.surfin.2020.100549

Korsunsky, A., McGurk, M., Bull, S., and Page, T., 1998. On the hardness of coated systems. Surface and Coatings Technology 99 (1- 2), 171- 183. doi:10.1016/S0257-8972(97)00522-7

Li, W., and Warren, R., 1993. A model for nano-indentation creep. Acta Metallurgica et Materialia 41 (10), 3065-3069. doi:10.1016/0956-7151(93)90119-D

Muthusamy, G., Wagstaff, S., and Allanore, A., 2020. Effect of Cooling Rate During Solidification of Aluminum–Chromium Alloy. The Minerals, Metals & Materials Series: Light Metals 2020, 204- 209. doi:10.1007/978-3-030-36408-3_28

Nix, W. D., and Gao, H., 1998. Indentation size effects in crystalline materials: A law for strain gradient plasticity. Journal of the Mechanics and Physics of Solids 46 (3), 411- 425. doi:10.1016/S0022-5096(97)00086-0

Okugawa, M., Ohigashi, Y., Furishiro, Y., Koizumi, Y., and Nakano, T., 2022. Equiaxed grain formation by intrinsic heterogeneous nucleation via rapid heating and cooling in additive manufacturing of aluminum-silicon hypoeutectic alloy. Journal of Alloys and Compounds 919, 1-6. doi:10.1016/j.jallcom.2022.165812

Puspitasari, P., Soepriyanto, O. R., Sasongko, M. I., Dika, J., and Doko, A. 2018. Mechanical and physical properties of aluminium-silicon (Al-Si) casting alloys reinforced by Zinc Oxide (ZnO). International Mechanical and Industrial Engineering Conference 2018, 204, 7. doi:10.1051/matecconf/201820405003

Shinde, D. M., and Sahoo, P., 2022. Nanoindentation, Scratch, and Corrosion Studies of Aluminum Composites Reinforced with Submicron B4C Particles. International Journal of Metalcasting 16 (3), 1363–1387. doi:10.1007/s40962-021-00692-7

Stroh, J., Sediako, D., Weiss, D., and Peterson, V. K., 2020. In Situ Neutron Diffraction Solidification Analyses of Rare Earth Reinforced Hypoeutectic and Hypereutectic Aluminum–Silicon Alloys. The Minerals, Metals & Materials Series: Light Metals 2020, 174- 178. doi:10.1007/978-3-030-36408-3_24

Tkatch, V. I., Limanovskii, A. I., Denisenko, S. N., and Rassolov, S. G., 2002. The effect of the melt-spinning processing parameters on the rate of cooling. Materials Science and Engineering A 323 (1- 2), 91- 96. doi:10.1016/S0921-5093(01)01346-6

Tutunchilar, S., Besharati Givi, M., Haghpanahi, M., and Asadi, P., 2012. Eutectic Al–Si piston alloy surface transformed to modified hypereutectic alloy via FSP. Materials Science and Engineering: A 534, 557-567. doi:10.1016/j.msea.2011.12.008

Uzun, O., Karaaslan, T., and Keskin, M., 2001. Production and Structure of Rapidly Solidified Al-Si Alloys. Turkish Journal of Physics 25(5), 455 – 466.

Uzun, O., Yilmaz, F., Emeksiz, C., Ergen, S., and Kolemen, U., 2018. Correlation of hardness and silicon morphology for Al-Si-Sb alloy. Archives of Metallurgy and Materials 63 (1), 467- 472. doi:10.24425/118963

Vijeesh, V., and Prabhu, K. N., 2014. Review of Microstructure Evolution in Hypereutectic Al–Si Alloys and its Effect on Wear Properties. Transactions of the Indian Institute of Metals 67 (1), 1- 18. doi:10.1007/s12666-013-0327-x

Zeren, M., and Karakulak, E., 2008. Influence of Ti addition on the microstructure and hardness properties of near-eutectic Al–Si alloys. Journal of Alloys and Compounds 450 (1-2), 255-259. doi:10.1016/j.jallcom.2006.10.131

Zhang, L., Zhan, Z., Jia, Y., Wang, W., and Zhou, B., 2007. Characterization of Al–Si–Mg alloys fast quenched from the melt by special medium. Journal of Materials Processing Technology 187- 188, 791- 793. doi:10.1016/j.jmatprotec.2006.11.110